Journal of Applied Polymer Science

Morphology and thermal degradation studies of melt-mixed PLA/PHBV biodegradable polymer blend nanocomposites with TiO_2 as filler

Julia P. Mofokeng, Adriaan S. Luyt*
Department of Chemistry, University of the Free State (Qwaqwa campus), Phuthaditjhaba 9866, South Africa
*Present address: Center for Advanced Materials, Qatar University, Doha, Qatar
Correspondence to: A. S. Luyt (LuytAS@qwa.ufs.ac.za or aluyt@qu.edu.qa)

ABSTRACT: The morphology and thermal stability of melt-mixed poly(lactic acid) (PLA)/poly(hydroxybutyrate-co-valerate) (PHBV) blends and nanocomposites with small amounts of TiO_2 nanoparticles were investigated. PLA/PHBV at 50/50 w/w formed a co-continuous structure, and most of the TiO_2 nanoparticles were well dispersed in the PLA phase and on the interface between PLA and PHBV, with a small number of large agglomerates in the PHBV phase. Thermogravimetric analysis (TGA) and TGA–Fourier-transform infrared spectroscopy was used to study the thermal stability and degradation behavior of the two polymers, their blends, and nanocomposites. The thermal stability of PHBV was improved through blending with PLA, whereas that of the PLA was reduced through blending with PHBV, and the presence of TiO_2 nanoparticles seemingly improved the thermal stability of both polymers in the blend. However, the degradation kinetics results revealed that the nanoparticles could catalyze the degradation process and/or retard the volatilization of the degradation products, depending on their localization and their interaction with the polymer in question. © 2015 Wiley Periodicals, Inc. J. Appl. Polym. Sci. **2015**, *132*, 42138.

KEYWORDS: biodegradable; blends; composites; degradation; kinetics

Received 16 November 2014; accepted 17 February 2015
DOI: 10.1002/app.42138

INTRODUCTION

In recent years, environmental pollution has become a great concern due to the high impact of plastic waste in daily use and the out-of-control emission of carbon dioxide into the atmosphere. Studies of bio-based and biodegradable polymers, more so from renewable resources, have attracted increased attention due to the great demand to reduce dependence on petroleum-based polymers which is the main source of plastic waste. Biodegradable polymers are believed to be an environmentally friendly replacement of the current petrochemical-based polymers. Recent interests in these biodegradable polymers are encouraged by the increasing cost of petroleum oil, as well as concerns for the environment and a shift toward sustainable manufacturing.[1–5] The applications of biodegradable polymers currently include mainly agriculture, biomedical, and food packaging applications. However, there is a large potential for many other applications such as automotive, aerospace, medical equipment, and various sanitary products.[6]

One of the most commonly used bio-based and biodegradable polymers, poly(lactic acid) (PLA), is produced by the ring-opening polymerization of lactide or the condensation polymerization of lactic acid monomers produced from renewable resources *via* a fermentation process.[7,8] Due to its commercial availability at a low cost, it has been broadly studied and used mainly for packaging and biomedical applications. PLA has good mechanical properties and biocompatibility, as well as thermoplasticity comparable to that of petrochemically derived polymers. It is known to degrade well when disposed along with municipal waste, so it is less of a burden to the environment.[2,3] Even though PLA is a very attractive biodegradable polymer, it cannot fully satisfy the requirements of industry. Disadvantages like poor melt properties, brittleness, and low thermal resistance limit its use in different applications. To overcome these problems, several methods were implemented and used to improve the lacking properties in PLA. These include blending with other biodegradable polymers, plasticization, and copolymerization. Among these methods, blending was reported to be the easiest and most cost effective.[9] Polymer blends had been extensively studied because it presents the possibility of enhancing the overall properties of the final material through a synergistic combination of the desirable properties of each component in one system.[10–12]

A range of renewable biodegradable polymers are currently available on the market, among others the polyhydroxyalkanoates (PHAs). The PHAs are a family of polyesters produced by microorganisms. The most common PHA is poly(hydroxybutyrate)

(PHB). Poly(hydroxybutyrate-co-valerate) (PHBV) is another PHA and is a co-polymer of PHB with randomly arranged 3-hydroxybutyrate and 3-hydroxyvalerate groups. This co-polymer was developed to improve PHB flexibility and thermal stability, and to lower its melting temperature and reduce its high crystallinity. PHBV has good flexibility and processing capabilities.[13]

Most polymer pairs are thermodynamically immiscible as a result of their unfavorable interaction. The macrophase separation and poor interfacial adhesion restrict property combination of the two components in the blend. In recent years, a new concept of compatibilization by using inorganic nanoparticles has been introduced. Unfortunately there are relatively few studies dealing with immiscible polymer blends whose interfaces are stabilized by solid particles.[14–17]

Nanometer inorganic compounds such as titanium dioxide (TiO_2), zinc oxide (ZnO), silica (SiO_2), aluminum dioxide (Al_2O_3), and silicon nitride (Si_3N_4) were tried as fillers in fabrics and polymers to improve the tribological properties. TiO_2 has received most of the attention because of its good thermal stability, accessibility, and catalytic properties. It is an inorganic material obtained from a variety of naturally occurring ores that contain ilmenite, rutile, anatase, and leucoxene, which are mined from deposits located throughout the world. It is generally used for various applications including photoelectrochemical activity, solar energy conversion, photocatalysis, UV detection, ultrasonic sensing, and as a promising material in applications such as water or wastewater treatment. Environmental compatibility, nontoxicity, and low price are some practical advantages of TiO_2.[18–23]

Few studies reported on the selective localization of inorganic nanoparticles in one of the phases in a polymer blend, or at the interface between the two polymers. The filler will selectively locate itself in order to reduce interfacial tension free surface energy, and as a result it may improve the interfacial interaction between the two polymers. This selective localization of the filler is mainly the result of the large difference in the affinity between the filler and the two matrix components. Thermodynamically the filler will be expected to locate in the lower viscosity phase to balance the viscoelastic difference between the two matrix components, which will contribute to the compatibility and improve the desired final properties. This assumption is based on entropy effects, where the entropy will be higher in the lower viscosity polymer in the molten state due to ease of chain movement. The nanoparticles should therefore disperse more easily in the lower viscosity polymer. It has also been reported that lower viscosity polymers has the ability to accommodate higher filler volumes.[24] Wu *et al.*[17,25] introduced multi-walled carbon nanotubes (MWCNTs) into a 30 : 70 w/w PLA/PCL blend. They found that the MWCNTs were selectively dispersed in the lower viscosity PCL phase and on the interface. They explained that such a selective localization of the MWCNTs not only prevented the coalescence of the discrete PLA phase, but also enhanced the interfacial adhesion. In this case, the MWCNTs acted as nanoreinforcement and compatibilizer, simultaneously improving the morphology and final properties of the PLA/PCL blend. If the filler is located at the interface of the two components, it can to some degree reduce the overall free energy of blending, leading to a thermodynamically driven compatibility. The localization of the filler is important to the final morphology and property control of immiscible blends.

Young's equation, eq. (1), is used to predict selective particle distribution in a polymer blend by calculating the wetting coefficient (ω_α).[26]

$$\omega_a = \frac{\gamma_{\text{PolymerB-Filler}} - \gamma_{\text{PolymerA-Filler}}}{\gamma_{\text{PolymerA-PolymerB}}} \quad (1)$$

where $\gamma_{\text{polymerB–Filler}}$ is the interfacial tension between polymer B and the filler, $\gamma_{\text{polymerA–Filler}}$ is the interfacial tension between polymer A and the filler, and $\gamma_{\text{polymerA–PolymerB}}$ is the interfacial tension between polymers A and B. The value of the wetting coefficient is normally used to determine where the filler is likely expected to disperse. If $\omega_\alpha < -1$, the particles are predicted to be localized in polymer B; if $\omega_\alpha > 1$, they are dispersed in polymer A; and if the value of ω_α is between -1 and 1, the nanoparticles are likely dispersed on the interface between the two polymers in the blend.[12] In rare cases where the particles are dispersed in both the interface and one of the phases, the third condition does not apply, so that a negative ω_α indicates dispersion of the particles in polymer B as well as the interface, and a positive ω_α indicates dispersion of the particles in polymer A and on the interface.[27,28]

Both PLA and PHBV are biodegradable polymers. Blending of PLA with PHBV could provide a practical way of improving or tailoring the structure and properties of the material, without compromising the biodegradability. Another important aspect of blending these two polymers is that the crystallinity of the blend will be improved since PHBV is highly crystalline when compared to PLA. A number of studies reported on the preparation of PLA/PHBV blends by solvent casting processes. This method was reported to improve the intimacy between the components in the blends. Although it has the important advantage of improving the mixing and interaction between the components in a blend, solution mixing is a very expensive method for preparation of blend samples, and it is not industrially viable because solvents are expensive and difficult to dispose of in an environmentally friendly way. Therefore, the use of melt-mixing is considered as a more acceptable way of sample preparation.[10,29–33]

In this article, the effect of blending of PLA with PHBV in the presence of TiO_2 nanoparticles as filler on the thermal stability and degradation behavior of PLA/PHBV/TiO_2 nanocomposites was studied. The structure and properties of the blend nanocomposites were also studied and related to the thermal behavior of the samples.

EXPERIMENTAL

Materials

The PLA used in the study is a commercial grade (PLA 2002D), obtained from Natureworks, LLC. (USA). It has a D-isomer content of 4%, a density of 1.24 g cm^{-3}, a glass transition temperature of ~53°C, and a melting temperature of ~153°C, with a degree of crystallinity of 33%. The PHBV biopolymer used was purchased from Goodfellow, Huntington, UK with a 12% PHV

content, density of 1.25 g cm^{-3}, a melting temperature of ~150°C, and a degree of crystallinity of 59%. Anatase titanium(IV)oxide (TiO_2) with particle sizes <25 nm and 99.7% purity was supplied by Sigma-Aldrich.

Preparation Method

The samples were prepared *via* melt-mixing using a Brabender Plastograph. PLA and PHBV were dried in an oven at 80°C for 4 h prior to mixing, and TiO_2 was used as received. 30/70, 50/50, and 70/30 w/w PLA/PHBV blends and their nanocomposites with 1, 3, and 5 wt % of TiO_2 were mixed at 170°C for 10 min. The samples were compression molded into 2-mm-thick sheets at the same temperature for 5 min using a hydraulic press at a pressure of 50 bar.

Characterization

Size exclusion chromatography (SEC) measurements were performed on a PL Olexis column (Polymer Laboratories). Chloroform was used as mobile phase at a flow rate of 1.00 mL min^{-1}. The samples were prepared at a concentration of 2 mg mL^{-1}. The column was calibrated with polystyrene standards from Polymer Laboratories (Church Stretton, Shropshire, UK). The chromatograph comprised a Waters 1515 isocratic pump, a Waters inline degasser AF, and a Waters 717 Plus auto sampler with a 100 μL sample loop. The system was connected to an evaporative light scattering detector (ELSD) (PL-ELS 1000). Nitrogen was used as carrier gas in the ELSD, at a flow rate of 1.5 SLM. The evaporator and nebulizer temperatures were set at 100 and 40°C, respectively.

The melt flow index of the two polymers in the blend was determined using a CEAST Melt Flow Junior. Ten samples each of both polymers were analyzed at 180°C. The amount of sample which flowed through the die over a period of 10 min under 2.16 kg was determined in each case.

Differential scanning calorimetry was used to determine the polymers' degree of crystallinity. The analyses were performed under nitrogen flow (20 ml min^{-1}) from 0 to 170°C at 10°C min^{-1}. The melting enthalpies of the polymers were determined, and eq. (2) was used to calculate their crystallinities.

$$X_C(\%) = \left(\frac{\Delta H_m}{\Delta H_m^o}\right) \times 100\% \quad (2)$$

where ΔH_m is the melting enthalpy and $\Delta H_m{}^0$ is the melting enthalpy of the 100% crystalline polymer. Values of 93.7[3] and 109 J g^{-1},[3,31] were used for PLA and PHBV respectively.

A Tescan VEGA3 scanning electron microscope (SEM) was used to study the surface dispersion of the TiO_2 nanoparticles in the PLA/PHBV blends. The liquid nitrogen fractured samples were spatter coated with gold for 30 s to eliminate sample charging, and analyses were performed at three different magnifications.

The morphologies of the nanocomposites were characterized by transmission electron microscopy (TEM). Images were obtained using a 200 kV FEI Tecnai 20 TEM fitted with Gatan Tridiem. The 50/50 w/w PLA/PHBV blend with 5 wt % TiO_2 nanoparticles was trimmed and sectioned to fit the ultramicrotome, since they were hard enough to cut without cooling. Thin sections of 100–150 nm were collected on copper grids and viewed. Staining was not necessary as the different phases could easily be distinguished. For TEM-energy dispersive spectrometry (EDS) analyses, the samples were sectioned at 150 nm using a Leica UC7 (Vienna, Austria) ultramicrotome, and examined with a Philips (FEI) (Eindhoven, The Netherlands) CM100 transmission electron microscope at 60 keV. EDS spectra were obtained with an Oxford X-Max (80 mm^2) analyzer (Wycombe, UK).

The contact angles of the neat polymers were determined on a surface energy evaluation system, based on the sessile drop method. At least 5 replicates were analyzed for each sample to ensure reproducibility of the results. The contact angles and surface energies of TiO_2 were acquired from the literature.[34] Distilled water (H_2O), and diiodomethane (CH_2I_2) were used as polar and nonpolar solvents, respectively. The literature values of their surface energies are (H_2O: $\gamma^p = 50.7$ mJ m^{-2} and $\gamma^d = 22.1$ mJ m^{-2}; CH_2I_2: $\gamma^p = 6.7$ mJ m^{-2} and $\gamma^d = 44.1$ mJ m^{-2}). The contact angles, total surface energies, as well as their dispersive and polar surface components were calculated using the Owens–Wendt method [eqs. (3) and (4)].[12,34,35]

$$\gamma_s = \gamma_s{}^d + \gamma_s{}^p \quad (3)$$

$$\gamma_1(1+\cos\theta) = \sqrt[2]{\gamma_s{}^d \cdot \gamma_l{}^d + \gamma_s{}^p \cdot \gamma_l{}^p} \quad (4)$$

where θ is the contact angle, γ is the surface energy, the subscripts 's' and 'l' indicate solid and liquid, respectively, while 'd' and 'p' indicate the dispersive and polar components, respectively. If the contact angle of at least two liquids, usually a polar and nonpolar with known $\gamma_l{}^d$ and $\gamma_l{}^p$ values, are measured on a solid surface, the $\gamma_s{}^d$ and $\gamma_s{}^p$ and the total surface energy (γ_s) of the solid can be calculated by combining eqs. (3) and (4).[36] The interfacial tensions between the components in a blend were calculated from the contact angle measurement results using the geometric mean equation (Equation (5)).[12,27]

$$\gamma_{12} = \gamma_1 + \gamma_2 - \sqrt[2]{\gamma_1^d \cdot \gamma_2^d + \gamma_1^p \cdot \gamma_2^p} \quad (5)$$

where γ_{12} = interfacial tension between components 1 and 2 in the blend, γ_1 and γ_2 are the total surface energies of components 1 and 2, $\gamma_1{}^d$ and $\gamma_2{}^d$ are the dispersive surface energies of components 1 and 2, and $\gamma_1{}^p$ and $\gamma_2{}^p$ are the polar surface energies of the components in the nanocomposites.

A Perkin-Elmer STA6000 thermogravimetric analyzer (TGA) was used to analyze the thermal degradation behavior of the samples. The analyses were done from 30 to 600°C at a heating rate of 10°C min^{-1} under nitrogen flow (20 ml min^{-1}). The sample masses were ~24 mg. The samples for thermal degradation kinetics were run at 3, 5, 7, 9, and 15°C min^{-1} heating rates under nitrogen atmosphere, and the TGA's integrated kinetics software (based on the Flynn–Ozawa–Wall model [eq. (6)] was used to calculate the activation energies.

$$\ln\beta = c - 1.052\left(\frac{E_a}{RT}\right) \quad (6)$$

where β is the heating rate in K min^{-1}, c, a constant, E_α, activation energy in kJ mol^{-1}, R, universal gas constant, and T, temperature in K. The plot of ln β vs $1/T$, obtained from the TGA curves recorded at several heating rates, should be a straight

Table I. Summary of Molar Masses, Melt Flow Index, and Surface Properties of PLA, PHBV, and Titania

	Contact angle (°)		Surface energy (mN m^{-1})			Molar mass (g mol^{-1})			
	H_2O	CH_2I_2	γ	γ^d	γ^p	M_n	M_w	D	MFI (g/10 min)
PLA	44.7 ± 1.0	35.4 ± 0.0	62.0	41.8	20.2	55,047	142,500	2.6	2.8
PHBV	54.7 ± 0.5	35.6 ± 0.7	56.3	41.7	14.6	36,710	77,537	2.1	8.1
TiO_2	19.7	10.1	80.7	46.4	34.3				

γ, surface energy; γ^d, dispersive component of surface energy; γ^p, polar component of surface energy; M_n, number average molar mass; M_w, weight average molar mass; *D*, dispersity index; MFI, melt flow index.

line. The activation energy was evaluated from its slope. The TGA was also connected to a Perkin-Elmer Spectrum 100 Fourier-transform infrared (FTIR) spectrometer to analyze the thermal degradation volatiles. The same temperature range and heating rate were used, and the volatiles were transferred to FTIR by a Perkin-Elmer TL 8000 balanced flow FT-IR EGA system at 200°C and a flow rate of 150 ml min^{-1}. Spectra were collected at five different temperatures during the degradation process.

RESULTS AND DISCUSSION

Molar Mass Analysis by SEC

The SEC results in Table I show that PLA has a higher molar mass and dispersity than PHBV. These results will be used later in this article when the morphologies of the blend nanocomposites are discussed.

Morphology

Figure 1 shows the SEM micrographs of the 50/50 w/w PLA/PHBV blend nanocomposites with 5 wt % TiO_2. In order to achieve good material properties, the reinforcement or filler should be well dispersed and should have good interaction with the matrix. In this system, no chemical interaction was expected, so only physical interactions were studied. The small particulate objects (shown with arrows and in the circle in Figure 1) are TiO_2 nanoparticles in the blend; they seem to be well dispersed and embedded in the polymer matrices.

Most polymer blends are thermodynamically immiscible, and consequently a multiphase phase morphology is usually observed. The two polymers can be clearly distinguished in Figure 2, and a co-continuous morphology is observed. The darker phase in the TEM photos is PHBV, and the TiO_2 nanoparticles are clearly visible. They are well dispersed in the PLA phase and on the PLA–PHBV interface, with some agglomerates. A very small number of agglomerates are visible in the PHBV phase. One would expect this selective localization of the nanoparticles in the PLA phase, and on the interface between PLA and PHBV, to be the result of the difference in molar mass, viscosity, and crystallinity of these two polymers. According to the SEC results in Table I, the PLA has a higher molar mass and a much higher melt viscosity (lower melt flow index) than PHBV. The nanoparticles would be expected to diffuse into the lower viscosity polymer in order to balance the viscoelastic properties. In this case, however, the nanoparticles are dispersed in the PLA phase. The crystallinity difference between the polymers could have been the driving force for the nanoparticles to select a polymer, since the inorganic nanoparticles would tend to locate

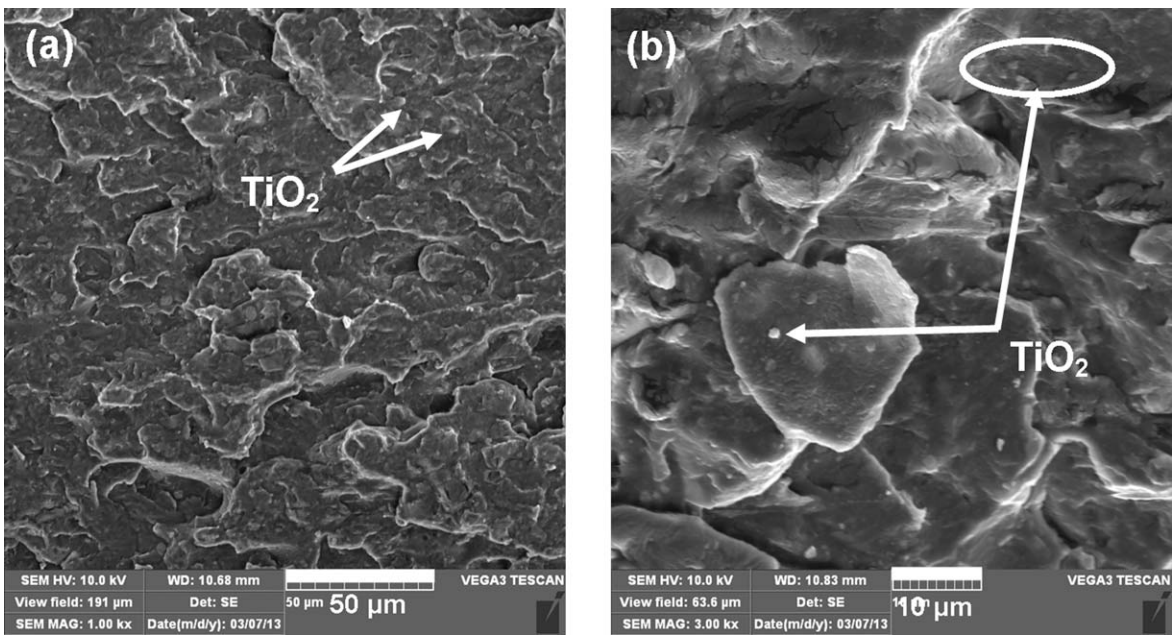

Figure 1. SEM micrographs of 50/50 w/w PLA/PHBVwith 5 wt % TiO_2 at (a) 1000× and (b) 3000× magnifications.

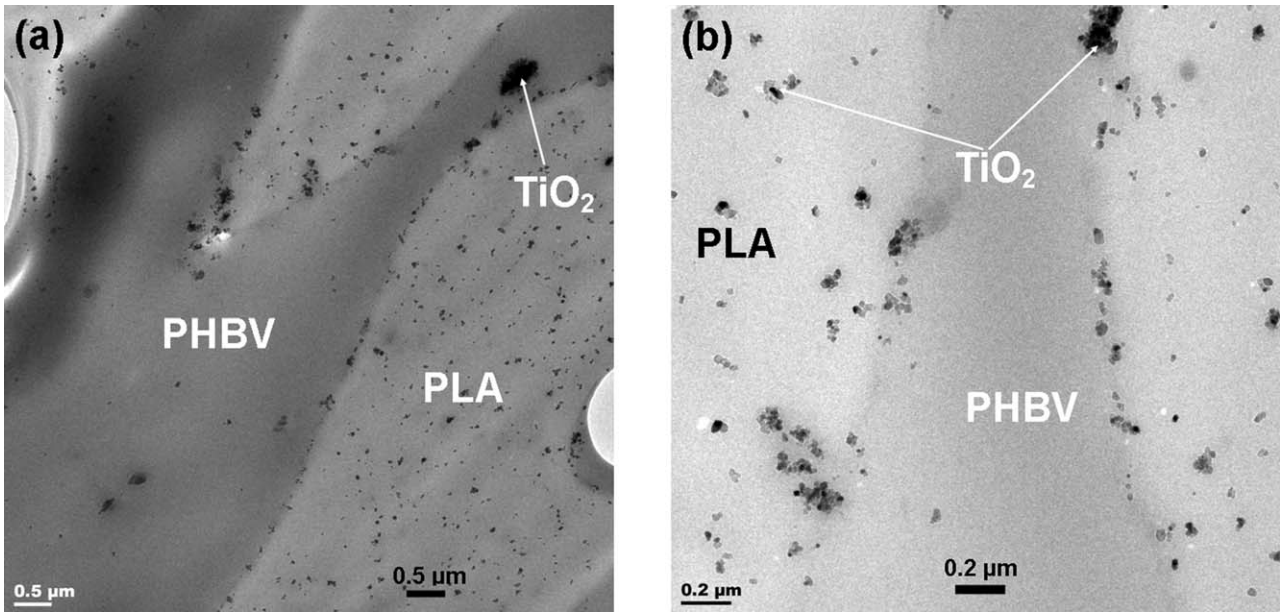

Figure 2. TEM micrographs of 50/50 w/wPLA/PHBV with 5 wt % TiO_2 at (a) 5700× and (b) 19000× magnifications.

themselves in the amorphous phase of a polymer. The PLA with its lower crystallinity (33% compared to 59% for PHBV) will in this respect be better suited as matrix for the nanoparticles. Another factor that could have influenced the selective localization of the nanoparticles is the difference in the surface energy between the components in the nanocomposite. If there are no specific interactions, this should determine how strong the nanoparticles will interact with a specific polymer. In this case, the PLA has a surface energy (62.0 mN m^{-1}) which is closer to that of TiO_2 (80.7 mN m^{-1}) than PHBV (56.3 mN m^{-1}), and the polar characters of PLA and TiO_2 (20.2 and 34.3 mN m^{-1}, respectively) are closer to each other than those of PHBV and TiO_2 (14.6 and 34.3 mN m^{-1}) (see Table I).

TEM-***EDS*** analysis of the blend nanocomposite clearly shows that the filler is finely dispersed in the PLA phase, while some large agglomerates are visible in the PHBV phase (Figure 3). Figure 3(a) shows a continuous PLA phase with the PHBV phase dispersed in it, although the morphology is clearly close to co-continuity. The EDS elemental analysis [Figure 3(b)] shows that there is no dispersed titania in the PHBV phase (solid ellipse), but only large agglomerates (dashed ellipse) that are almost pure titania, while the PLA phase clearly contains titania which is visible as small, finely dispersed particles (dotted ellipse). These particles also form a well-defined border on the interface between the two polymers [see arrows in Figures 3(b,c)].

The wetting coefficient model[12,26–28] was applied to confirm the TEM and TEM-EDS results. The contact angles and surface energies of PLA, PHBV, and TiO_2 are presented in Table I, and the interfacial tensions and wetting coefficient are summarized in Table II. The wetting coefficient value of 5.09 indicates that the nanoparticles should be situated in PLA and maybe on the interface. There are two factors involved in determining the selective localization of the TiO_2 nanoparticles in a two-phase polymer blend, and those are thermodynamic and kinetic effects. Thermodynamically the particles interact more favorably with one of the polymers in order to decrease the system's free energy, and they will tend to locate in such a way to minimize the interfacial tension between the polymers, and hence improve the interfacial adhesion between the two phases. This happens mostly when the particles are located at the interface between the two components.[25] At equilibrium, the particles will likely disperse in the phase where the affinity between the polymer and the nanoparticles is high. The calculated interfacial tensions from the surface energy results indicate that the interfacial tension between PHBV and TiO_2 (4.27 mN m^{-1}) is higher than that between PLA and TiO_2 (1.98 mN m^{-1}). This explains why they preferably disperse in the PLA phase.

Thermodymically, melt-mixing of the two polymers with a significant difference in molar mass, viscosity, and crystallinity would give rise to the selective localization of the third component, which is TiO_2 nanoparticles in this case. PLA has a higher molar mass and viscosity than PHBV (Table II). One would therefore expect the TiO_2 nanoparticles to more easily disperse in the PHBV phase, which is not the case as could be seen from the TEM and TEM-EDS results. However, differences in crystallinity could have played a role. Although both polymers are completely amorphous in the molten state where mixing takes place, it would be expected that during cooling when the polymers crystallize, the nanoparticles would be forced out of the more highly crystalline polymer because they would preferably tend to be in the amorphous phase of a polymer, unless the interaction between the nanoparticles and the polymer is strong enough that the nanoparticles can act as nucleating sites for the polymer. Because of the much higher crystallinity of PHBV and the much lower interfacial tension between PLA and TiO_2, it

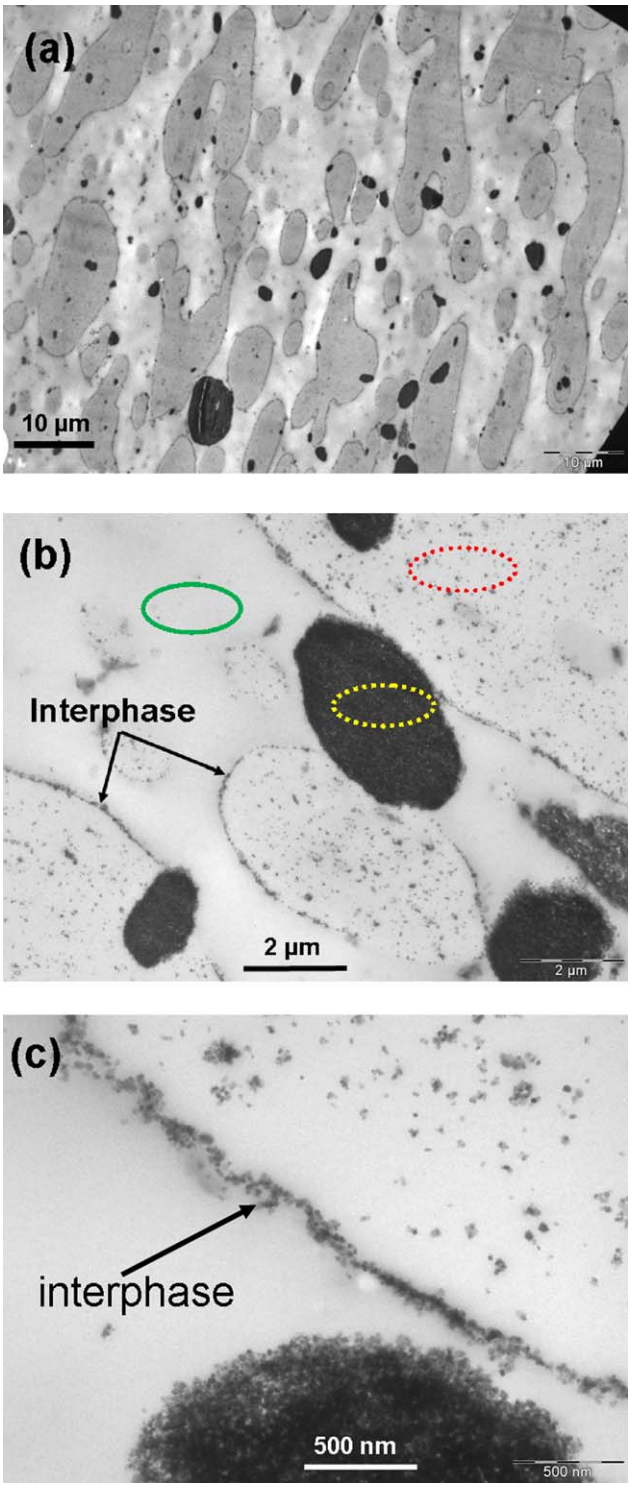

Figure 3. TEM-EDS micrographs of 50/50 w/wPLA/PHBV with 5 wt % of TiO_2 to illustrate the localization of nanoparticles in the different phases of the blend, showing (a) the morphology, (b) positions for the elemental analyses, and (c) a detailed view of the filler particle distribution. [Color figure can be viewed in the online issue, which is available at wileyonlinelibrary.com.]

could be expected with some certainty that the nanoparticles would locate in the PLA phase and even to some extent act as nucleation sites for the crystallization of PLA. The strong interfacial tension between PHBV and TiO_2 also explains the large nanoparticles agglomerates in the PHBV phase because the nanoparticles clearly have a higher affinity for each other than for the PHBV chains, and the melt-mixing torque was probably not enough to break up these agglomerates and redisperse the particles in the PLA phase and on the interface. The relatively high melt viscosity of PLA, and the not-so-low PLA–TiO_2 interfacial tension, to some extent explains why a large number of nanoparticles are located at the PLA/PHBV interface.

Thermogravimetric Analysis

The good distribution of the filler in one of the polymers and on the interface should improve some properties in the PLA/PHBV blend nanocomposites, one of which is the thermal stability. Thermal degradation will reduce the usability of a polymer, especially in the case of recycling where the polymer undergoes several cycles of high and low temperatures. We used TGA and thermal degradation kinetics analyses to study the thermal degradation of the blends and their nanocomposites. Figures 4–6 show the effect of varying filler content on the mass loss curves of the blends at constant PLA/PHBV ratios. It is clear that the two polymers degrade separately, confirming their immiscibility. The temperature for 50% PHBV degradation was 280°C, while that for 50% PLA degradation was 364°C. This difference in thermal stability of PLA and PHBV is due to the structural difference between the two polymers. The PLA degradation proceeds according to a back-biting ester interchange reaction which takes place through a nonradical mechanism involving the –OH chain ends. The products vary with the reaction point in the backbone and can be lactide molecules, oligomeric rings, or acetaldehyde plus carbon monoxide. The thermal degradation of PHBV follows a random chain scission mechanism involving a β-hydrogen elimination process (six-membered ring ester decomposition process) to form substrate olefins and oligomers.[10,37]

The thermal stability of PHBV observably improved (temperature at which 50% polymer degraded increased from about 280 to about 291°C) with an increase in PLA content in the blends, and further increased to 302°C in the presence of the nanoparticles; this is because PLA and TiO_2 also absorb heat energy and because they have higher thermal stabilities than PHBV, they insulate the PHBV so that it starts to degrade at higher temperatures. On the other hand, the temperature at 50% mass loss of PLA decreased from 364 to 349°C with increasing PHBV content in the blend, but again increased to the same level as that of pure PLA with increasing nanoparticle content. The influence of the nanoparticles on the thermal stabilities of the polymers can be attributed to the shielding effect of the nanoparticles,[37,38] and/or a retardation effect of the nanoparticles on the movement of free radicals and volatile degradation products.[34] This becomes clear when comparing the extent to which the thermal stability of the two polymers improved in the presence of TiO_2. The increase in degradation temperature was more significant in the case of PLA, which can be explained by the fact that nanosized particles were well dispersed in PLA which resulted in stronger and more effective interaction compared to PHBV. The residue percentage at 400°C is about 1.5% for all the blends, which indicates a low level of char formation by the polymers

Table II. Interfacial Tensions and Wetting Coefficient of the Investigated Materials

Component couple	Interfacial tension/mN m^{-1} and wetting coefficient
PLA/PHBV	0.45
PLA/TiO_2	1.98
PHBV/TiO_2	4.27
ω_α	5.09

ω_α, wetting coefficient.

themselves. If this percentage is subtracted from the values observed for the blend nanocomposites, the differences are almost exactly equal to the amount of titania originally mixed into the blends. This indicates a fair dispersion of the filler in the blends, as was observed from the morphological analysis.

Figures 7 and 8 show the temperatures at 50% degradation of each component in the blends as function of titania content in the nanocomposites. These figures represent both the effect of blending and filler loading on the thermal stability of each polymer in the blends. Figure 7 was plotted with the temperatures calculated from the thermal degradation step of PHBV, and it clearly shows that when the PLA content increases the thermal stability of PHBV also increases, and that the stability even further improves with an increase in filler content. The degradation of PLA, on the other hand, decreases with increasing PHBV content, but the filler has a much stronger stabilizing effect on the degradation of PLA (Figure 8). This is a typical example where blending averages the properties of the two polymers in the blend, and where a well-dispersed inorganic filler retards the degradation of the polymer matrix in which it is dispersed. As discussed earlier, there are more filler particles well dispersed in the PLA, and therefore the filler has a stronger stabilizing effect on PLA degradation than on PHBV degradation.

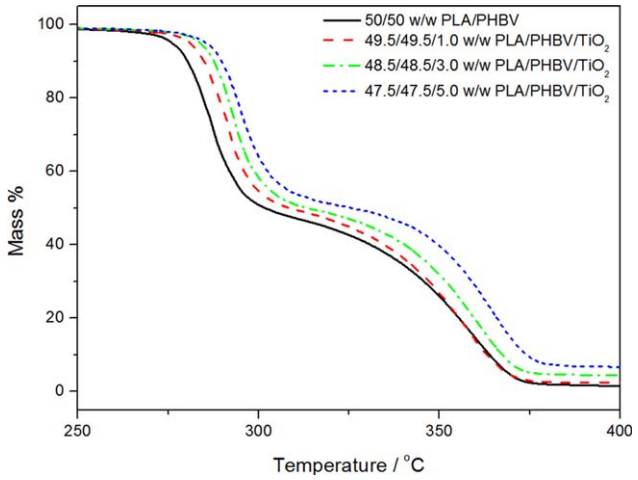

Figure 5. TGA curves of 50/50 w/w PLA/PHBV with different amounts of TiO_2. [Color figure can be viewed in the online issue, which is available at wileyonlinelibrary.com.]

Degradation Kinetics

Degradation kinetics analyses may assist in explaining the degradation behavior of the polymers in the different samples. Figures 9–16 show the degradation kinetics results for the individual polymers without and with filler, and of their blends without and with TiO_2. The activation energy (E_α) of degradation of PLA slightly increased with extent of degradation at low conversions, but decreased quite significantly as the degradation proceeded (Figure 9). This indicates an auto-acceleration effect as the degradation progresses. In the presence of TiO_2, PLA has much lower activation energies of degradation, probably because of a catalytic effect of the nanoparticles on the PLA degradation.[39,40] It does, however, still show the initial increase followed by a decrease toward higher extents of degradation. This seems to be contrary to the fact that the presence of TiO_2 nanoparticles retarded the PLA degradation, as was indicated by the TGA results. However, it is quite possible that less energy is needed to initiate the degradation in the presence of titania

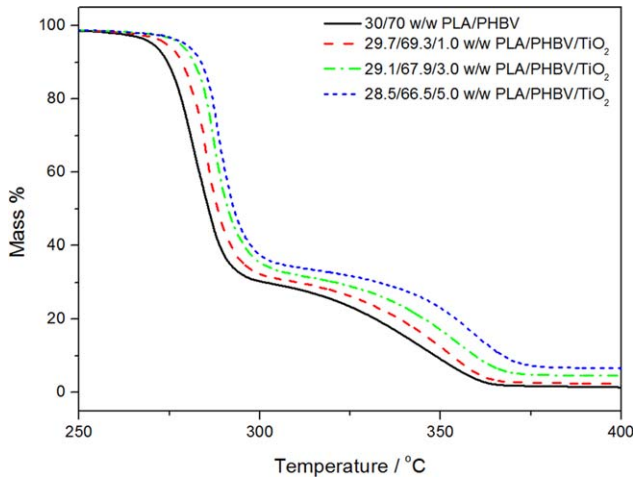

Figure 4. TGA curves of 30/70 w/w PLA/PHBV with different amounts of TiO_2. [Color figure can be viewed in the online issue, which is available at wileyonlinelibrary.com.]

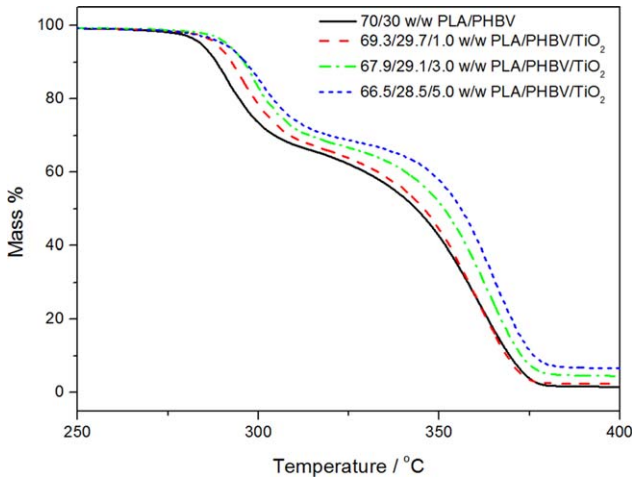

Figure 6. TGA curves of 70/30 w/w PLA/PHBV with different amounts of TiO_2. [Color figure can be viewed in the online issue, which is available at wileyonlinelibrary.com.]

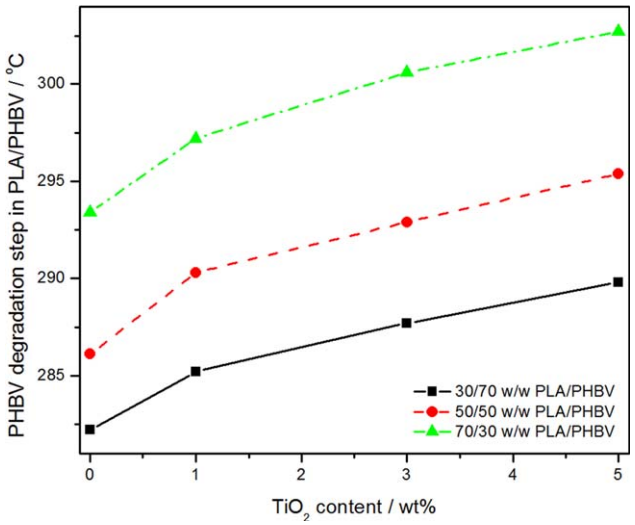

Figure 7. Effect of blending and filler addition on the temperature at 50% mass loss of PHBV in the PLA/PHBV blends and nanocomposites. [Color figure can be viewed in the online issue, which is available at wileyonlinelibrary.com.]

nanoparticles, but that the nanoparticles may retard the diffusion of the volatile degradation products out of the polymer, so that the onset of mass loss is at a higher temperature for the PLA nanocomposite.[39,40] As can be seen in Figure 10, the mass loss rate (slope of the mass loss step) is steeper for the nanocomposite, which means that the evolution of the volatile degradation products was faster after the onset of mass loss. Comparison of the FTIR spectra in Figure 11 clearly shows much lower intensities for the CO_2 peaks between 2300 and 2400 cm^{-1}, the –C=O vibration at about 1785 cm^{-1}, and the –C-O-C at about 1120 cm^{-1} between the spectra at comparable temperatures for the PLA in the nanocomposite compared to those for neat PLA. The carbonyl peak for the nanocomposite is

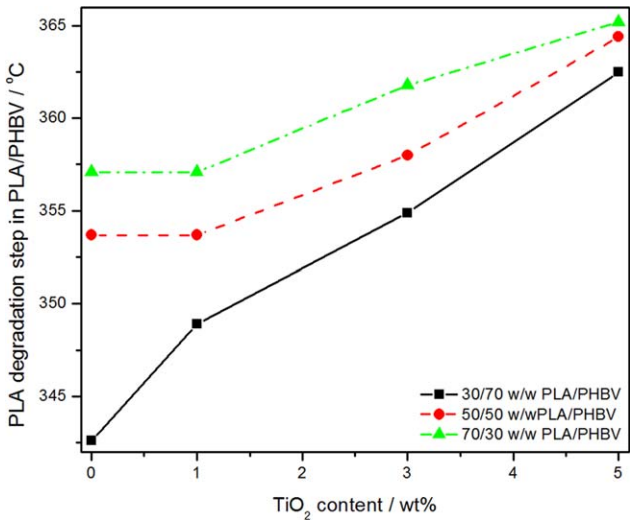

Figure 8. Effect of blending and filler addition on the temperature at 50% mass loss of PLA in the PLA/PHBV blends and nanocomposites. [Color figure can be viewed in the online issue, which is available at wileyonlinelibrary.com.]

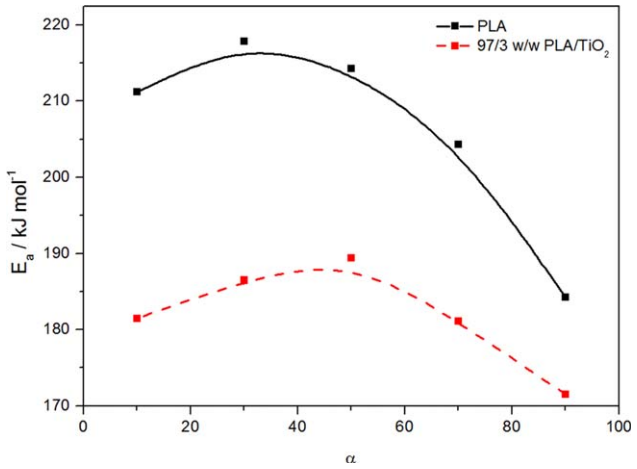

Figure 9. Activation energy vs. extent of degradation for PLA and PLA in the 97/3 w/w PLA/TiO_2 nanocomposite. [Color figure can be viewed in the online issue, which is available at wileyonlinelibrary.com.]

also at a lower wavenumber (1762 cm^{-1}) than that for neat PLA (1789 cm^{-1}). Both these observations are strong indications that the degradation products interacted with the nanoparticles, and that their volatilization has been retarded as a result of this.

The activation energy of degradation of PHBV remained unchanged around 146 kJ mol^{-1} throughout the degradation process (Figure 12). This could mean that the degradation mechanism of pure PHBV did not change throughout the degradation process, which probably has a single rate-determining step because of the independence of E_α on the extent of degradation.[39] In the presence of TiO_2, the E_α started at 120 kJ mol^{-1} and increased almost linearly with increasing degradation to 135 kJ mol^{-1}. The decrease in activation energy of PHBV in the presence of TiO_2 nanoparticles is initially about 25 kJ mol^{-1}, which is attributed to the lowering of the thermal stability at the initial stages of degradation. This indicates that the TiO_2 nanoparticles probably catalyzed the degradation of

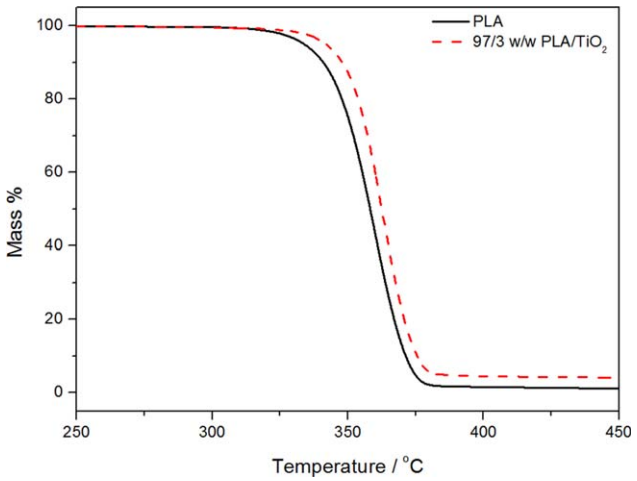

Figure 10. TGA curves of neat PLA and PLA in the 97/3 w/w PLA/TiO_2 nanocomposite. [Color figure can be viewed in the online issue, which is available at wileyonlinelibrary.com.]

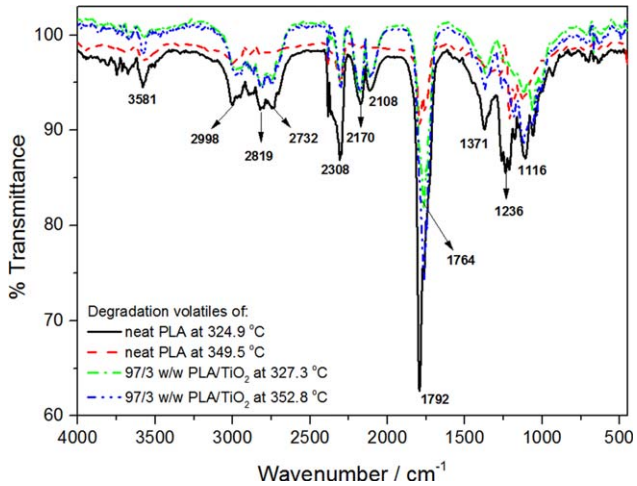

Figure 11. FTIR spectra of the degradation products of neat PLA and PLA in 97/3 w/w PLA/TiO_2. [Color figure can be viewed in the online issue, which is available at wileyonlinelibrary.com.]

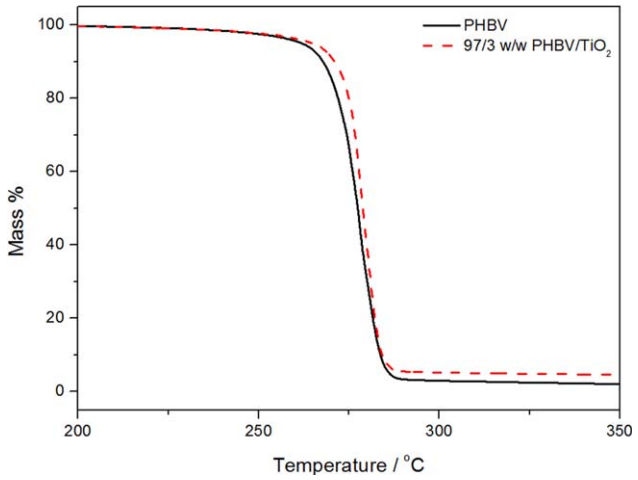

Figure 13. TGA curves of neat PHBV and PHBV in the 97/3 w/w PHBV/TiO_2 nanocomposite. [Color figure can be viewed in the online issue, which is available at wileyonlinelibrary.com.]

PHBV,[41,42] but that the effectiveness of this catalytic effect decreased with increasing extent of degradation, probably because the nanoparticles were much more agglomerated in PHBV than in PLA. It also seems as if the volatilization of the degradation products was initially retarded through interaction with the nanoparticles, because the onset of degradation for PHBV in the nanocomposite is clearly higher than that of neat PHBV, while the volatilization is clearly faster as can be seen from the slopes of the mass loss curves in Figure 13. The PHBV degradation products clearly did not interact so strongly with the nanoparticles as in the case of PLA, which is also clear from the FTIR spectra in Figure 14 that are almost identical for neat PHBV and PHBV in the nanocomposite at comparable temperatures. From these spectra, it is also clear that the presence of the nanoparticles did not change the PHBV degradation mechanism.

Figure 15 illustrates how E_α changed with extent of degradation for the 50/50 PLA/PHBV blend and the 47.5/47.5/5.0 w/w PLA/

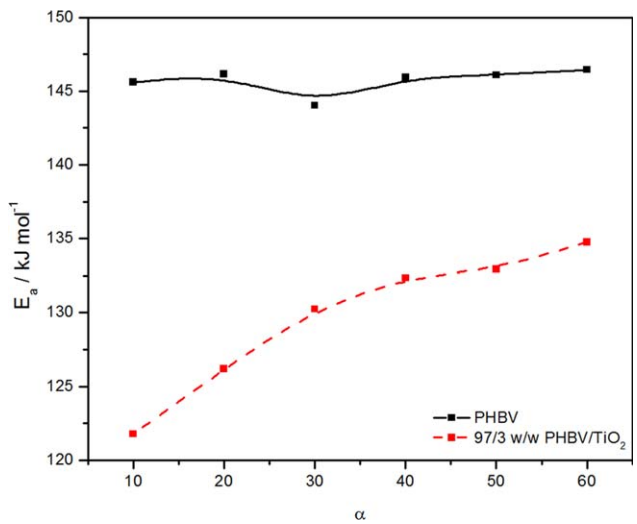

Figure 12. Activation energy vs. extent of degradation for PHBV and PHBV in the 97/3 w/w PHBV/TiO_2 nanocomposite. [Color figure can be viewed in the online issue, which is available at wileyonlinelibrary.com.]

PHBV/TiO_2 blend nanocomposite. The first part of the graph, up to about 47% mass loss, represents the activation energy for PHBV degradation. The rest of the graph represents the activation energy for PLA degradation. The E_α of the PHBV in the blend is slightly lower than that of the pure PHBV (Figure 12). However, the decrease in E_α of the PHBV in the PLA/PHBV blend nanocomposite is much less significant than that of PHBV in the PHBV nanocomposite. The reason is probably that all the nanoparticles were in contact with PHBV in the PHBV nanocomposite, even if agglomerated, while most of the nanoparticles were in the PLA phase or on the interface in the blend nanocomposites. In the presence of the nanoparticles, there is a very obvious decrease in the activation energy for PLA degradation, and the activation energy decreases with increasing extent of degradation, contrary to the increase observed for PLA in the blend. There is, however, not a clear-cut explanation for this observation. On the one hand, the nanoparticles can retard the evaporation of the volatile degradation products, while on the other hand, they may catalyze the degradation reaction. In this case it seems as if the catalysis effect is more dominant, and therefore the activation energy decreased with extent of degradation.

The spectra of the degradation volatiles in Figure 16 were taken at approximately 280°C (which falls within the PHBV degradation step) and 341°C (which falls within the PLA degradation step. The peaks at 1660 cm^{-1} (C=C stretching), 1755 cm^{-1} (C=O stretching), 3581 and 968 cm^{-1} (O-H vibrations), and the bands in the range of 1500–800 cm^{-1} (CH_3, CH bending vibrations, and the heavily overlapped C-O-C and C-C stretching vibrations) in the 280°C spectra (for the blend and the blend nanocomposite) indicate the presence of ester groups, carboxylic acids, and linear oligomers with crotonate end groups,[10,42,44–46] that are the expected products from the degradation of PHBV, in the volatiles. Except for differences in the peak intensities, there is no difference between the spectra for PLA/PHBV and PLA/PHBV/TiO_2. This confirms that the degradation mechanism was not influenced by the presence of the nanoparticles. We did not present the FTIR curves of the

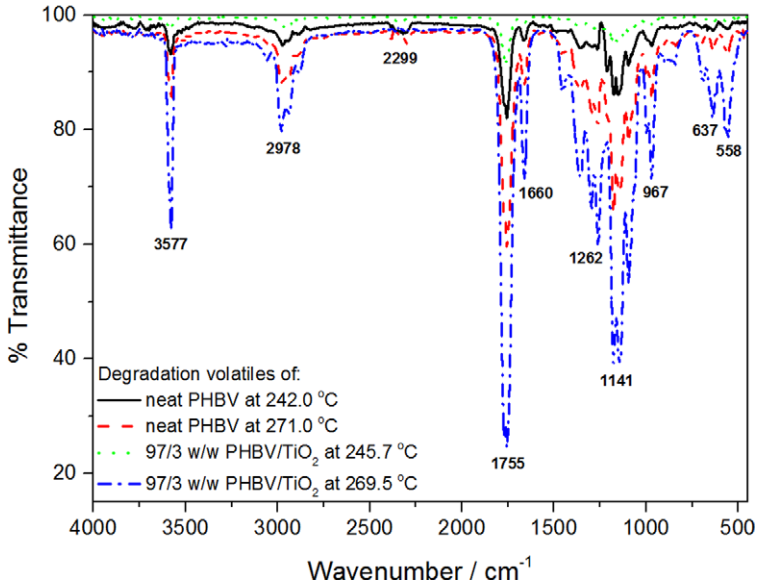

Figure 14. FTIR spectra of the degradation products of neat PHBV and PHBV in 97/3 w/w PHBV/TiO_2. [Color figure can be viewed in the online issue, which is available at wileyonlinelibrary.com.]

volatiles at different temperatures during the degradation process, but these results show that the peaks in the PLA/PHBV spectrum reached their maximum intensity at a 10°C lower temperature, which supports our previous observation that the TiO_2 nanoparticles probably interacted with the degradation volatiles and retarded their diffusion out of the sample.

The spectra obtained at a higher temperature of 342°C show peaks at 3580 cm^{-1} (O-H vibrations), 2997 and 2747 cm^{-1} (CH_2 stretching), 1766 cm^{-1} (C=O stretching), 1136 cm^{-1} (C-O-C stretching), and 2310 cm^{-1} (CO_2 vibrations), that are characteristic of lactide molecules, oligomeric rings, and acetaldehyde plus carbon monoxide, that are the previously determined degradation products of PLA.[10,37,43,46] In this case, there are also no differences between the spectra of PLA/PHBV and PLA/PHBV/TiO_2, confirming that the presence of the nanoparticles did not change the degradation mechanism. In this case, however, the maximum peak intensities were observed at a lower temperature for PLA/PHBV/TiO_2, which is in line with the catalytic effect of the nanoparticles on the degradation of PLA, as mentioned in our degradation kinetics discussion.

CONCLUSIONS

The purpose of this article was to investigate the influence of blending and the presence of small amounts of titania nanoparticles on the thermal degradation behavior of PLA and PHBV. The 50/50 w/w blend showed a co-continuous morphology, while the nanoparticles were selectively localized in the PLA phase and at the interface between PLA and PHBV. This was shown to be the result of differences in surface energies and interfacial tensions between the PLA, PHBV, and TiO_2, as well

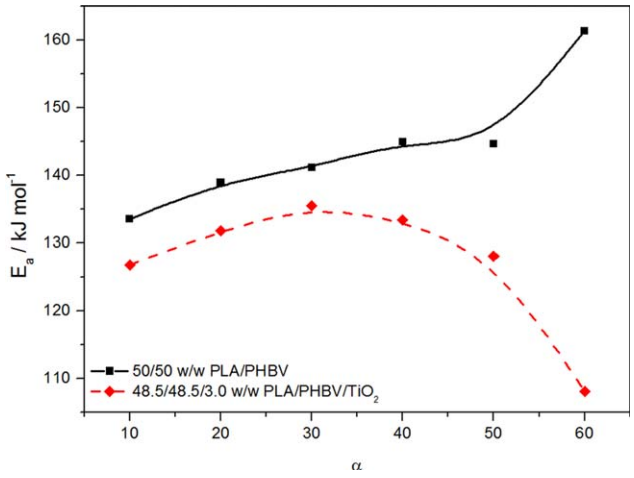

Figure 15. Activation energy vs. extent of degradation for a 50/50 w/w PLA/PHBV blend and its nanocomposite with 3 wt % TiO_2. [Color figure can be viewed in the online issue, which is available at wileyonlinelibrary.com.]

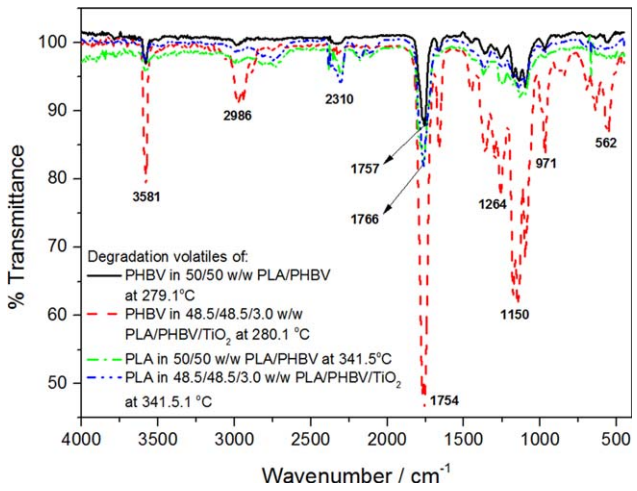

Figure 16. FTIR spectra of the degradation products of PHBV and PLA in 50/50 w/w PLA/PHBV and its nanocomposite with 3 wt % TiO_2. [Color figure can be viewed in the online issue, which is available at wileyonlinelibrary.com.]

as differences in the degree of crystallinity of PLA and PHBV. Blending of PLA with PHBV improved the thermal stability of PHBV, since PLA is more thermally stable, and the presence of the nanoparticles increased the mass loss temperatures of both polymers. This was, however, not necessarily an indication of better thermal stability because all indications are that the well dispersed and small nanoparticles in PLA catalyzed the degradation process, but also inhibited the diffusion of the degradation volatiles out of the sample. The same catalysis effect was not obvious in the case of PHBV, but the retardation of degradation product volatilization could also be seen in this case. It was further found that the presence of titania nanoparticles did not change the degradation mechanisms of the polymers.

ACKNOWLEDGMENTS

The authors would like to thank the South African National Research Foundation (NRF) for the financial support.

REFERENCES

1. As'habi, L.; Jafari, S. H.; Khonakdar, H. A.; Boldt, R.; Wagenknecht, U.; Heinrich, G. *eXPRESS Polym. Lett.* **2013**, *7*, 21.
2. Guan, Q.; Naguib, H. E. *J. Polym. Environ.* **2014**, *22*, 119.
3. Zhao, H.; Cui, Z.; Wang, X.; Turng, L. -S.; Peng, X. *Compos. B* **2013**, *51*, 79.
4. Ojijo, V.; Ray, S. S.; Sadiku, R. *Appl. Mater. Interfaces* **2012**, *4*, 6690.
5. Schwach, E.; Avérous, L. *Polym. Int.* **2004**, *53*, 2115.
6. Cava, D.; Gavara, R.; Lagarón, J. M.; Voelkel, A. *J. Chromatogr. A* **2007**, *1148*, 86.
7. Jamshidian, M.; Tehrany, E. A.; Imran, M.; Jacquot, M.; Desobry, S. *Comp. Rev. Food Sci. Food Saf.* **2010**, *9*, 552.
8. Signori, F.; Coltell, M. -B.; Bronco, S. *Polym. Degrad. Stab.* **2009**, *94*, 74.
9. Eslami, H.; Kamal, M. R. *J. Appl. Polym. Sci.* **2013**, *127*, 2290.
10. Nanda, M. R.; Misra, M.; Mohanty, A. K. *Macromol. Mater. Eng.* **2011**, *296*, 719.
11. Tokiwa, Y.; Calabia, B. P.; Ugwa, C. U.; Aiba, S. *Int. J. Mol. Sci.* **2009**, *10*, 3722.
12. Wu, D.; Lin, D.; Zhang, J.; Zhou, W.; Zhang, M.; Zhang, Y.; Wang, D.; Lin, B. *Macromol. Chem. Phys.* **2011**, *212*, 613.
13. Martínez-Sanz, M.; Villano, M.; Oliveira, C.; Albuquerque, M. G. E.; Majone, M.; Reis, M.; Lopez-Rubio, A.; Lagaron, J. M. *New Biotechnol.* **2014**, *31*, 364.
14. Si, M.; Araki, T.; Ade, H.; Kilcoyne, A. L. D.; Fisher, R.; Skolov, J. C.; Rafailovich, M. H. *Macromolecules* **2006**, *39*, 4793.
15. Elias, L.; Fenouillot, F.; Majeste, J. C.; Cassagnau, Ph. *Polymer* **2007**, *48*, 6029.
16. Elias, L.; Fenouillot, F.; Majeste, J. C.; Alcouffe, P.; Cassagnau, Ph. *Polymer* **2008**, *49*, 4378.
17. Laredo, E.; Grimau, M.; Bello, A.; Wu, D. F.; Zhang, Y. S.; Lin, D. P. *Biomacromolecules* **2010**, *11*, 1339.
18. Shi, Y.; Feng, X.; Wang, H.; Lu, X. *Wear* **2008**, *264*, 934.
19. Maurya, A.; Chauhan, P. *Polym. Bull.* **2012**, *68*, 961.
20. Shi, F.; Ma, Y.; Ma, J.; Wang, P.; Sun, W. *J. Memb. Sci.* **2012**, *389*, 522.
21. Nakayama, N.; Hayashi, T. *Polym. Degrad. Stab.* **2007**, *92*, 1255.
22. Chou, P. M.; Mariatti, M.; Zulkifli, A.; Sreekantan, S. *Compos. B* **2012**, *43*, 1374.
23. Shi, H.; Magaye, R.; Castranova, V.; Zhao, J. *Part. Fibre Toxicol.* **2013**, *10*, 1.
24. Cramer, N. B.; Stansbury, J. W.; Bowman, C. N. *Int. Am. Assoc. Dent. Res.* **2011**, *90*, 402.
25. Wu, D.; Zhang, Y.; Zhang, M.; Yu, W. *Biomacromolecules* **2009**, *10*, 417.
26. Zhao, B.; Fu, R. W.; Zhang, M. Q.; Yang, H.; Rong, M. Z.; Zheng, Q. *Polym. J.* **2006**, *38*, 799.
27. Wang, X.; Xu, K. -J.; Xu, X. -B.; Park, S. -J.; Kim, S. *J. Appl. Polym. Sci.* **2009**, *113*, 2485.
28. Fenouillot, F.; Cassagnau, P.; Majeste, J. C. *Polymer* **2009**, *50*, 1333.
29. Bledzki, A. K.; Jaszkiewicz, A. *Compos. Sci. Technol.* **2010**, *70*, 1687.
30. Modi, S.; Koelling, K.; Vodovotz, Y. *J. Appl. Polym. Sci.* **2012**, *124*, 3074.
31. Ferreira, B. M. P.; Zavaglia, C. A. C.; Duek, E. A. R. *J. Appl. Polym. Sci.* **2002**, *86*, 2898.
32. Miao, L.; Qiu, Z.; Yang, W.; Ikehara, T. *React. Funct. Polym.* **2008**, *68*, 446.
33. Cailloux, J.; Santana, O. O.; Franco-Urquiza, E.; Bou, J. J.; Carrasco, F.; Gámez-Pérez, J.; Maspoch, M. L. *eXPRESS Polym. Lett.* **2013**, *7*, 304.
34. Xiu, H.; Bai, H. W.; Huang, C. M.; Xu, C. L.; Li, X. Y.; Fu, Q. *eXPRESS Polym. Lett.* **2013**, *7*, 261.
35. Yang, H.; Zhang, X.; Qu, C.; Li, B.; Zhang, L.; Zhang, Q.; Fu, Q. *Polymer* **2007**, *48*, 860.
36. Owens, D.; Wendt, R. *J. Appl. Polym. Sci.* **1969**, *13*, 1741.
37. McNeill, I.; Leiper, H. *Polym. Degrad. Stab.* **1985**, *11*, 309.
38. Liao, H. -T.; Wu, C. -S. *J. Appl. Polym. Sci.* **2008**, *108*, 2280.
39. Vassiliou, A. A.; Chrissafis, K.; Bakiaris, D. N. *J. Therm. Anal. Calorim.* **2010**, *100*, 1063.
40. Majoni, S.; Su, S.; Hossenlopp, J. M. *Polym. Degrad. Stab.* **2010**, *95*, 1593.
41. Lin, H.; Han, L.; Dong, L. *J. Appl. Polym. Sci.* **2014**; 40480.
42. Yu, H. -Y.; Qin, Z. -Y.; Liu, Y. -N.; Chen, L.; Liu, N.; Zhou, Z. *Carbohydr. Polym.* **2012**, *89*, 971.
43. Lin, H.; Han, L.; Dong, L. *J. Appl. Polym. Sci.* **2014**, 40480.
44. Zhang, J.; Sato, H.; Noda, I.; Ozaki, Y. *Macromolecules* **2005**, *38*, 4274.
45. Liu, Q. -S.; Zhu, M. -F.; Wu, W. -H.; Qin, Z. -Y. *Polym. Degrad. Stab.* **2009**, *94*, 18.
46. Sato, H.; Murakami, R.; Padermshoke, A.; Hirose, F.; Senda, K.; Noda, I. *Macromolecules* **2004**, *37*, 7203.